JACS
JOURNAL OF THE AMERICAN CHEMICAL SOCIETY
Article
pubs.acs.org/JACS

Mechanistic Investigations of the Rhodium Catalyzed Propargylic CH Activation

Urs Gellrich,[†] Antje Meißner,[‡] Alberto Steffani,[†] Matthias Kähny,[†] Hans-Joachim Drexler,[‡] Detlef Heller,[‡] Dietmar A. Plattner,[†] and Bernhard Breit*[,†]

[†]Institut für Organische Chemie, Albert-Ludwigs-Universität, 79104 Freiburg, Germany
[‡]Leibniz-Institut für Katalyse, Universität Rostock, 18059 Rostock, Germany

Supporting Information

ABSTRACT: Previously we reported the redox-neutral atom economic rhodium catalyzed coupling of terminal alkynes with carboxylic acids using the DPEphos ligand. We herein present a thorough mechanistic investigation applying various spectroscopic and spectrometric methods (NMR, *in situ*-IR, ESI-MS) in combination with DFT calculations. Our findings show that in contrast to the originally proposed mechanism, the catalytic cycle involves an intramolecular protonation and not an oxidative insertion of rhodium in the OH bond of the carboxylic acid. A σ-allyl complex was identified as the resting state of the catalytic transformation and characterized by X-ray crystallographic analysis. By means of ESI-MS investigations we were able to detect a reactive intermediate of the catalytic cycle.

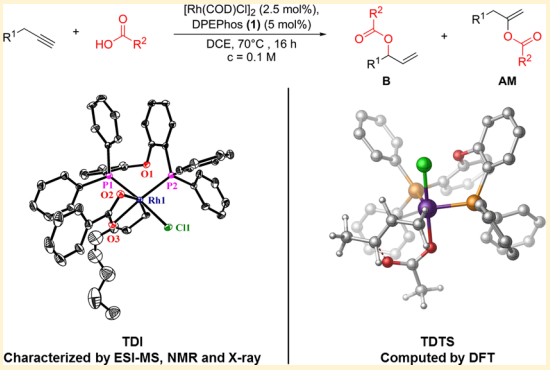

INTRODUCTION

Allylic alcohols and the corresponding ester derivatives are valuable building blocks in organic synthesis.[1] A large number of methods to access these compounds are known, including asymmetric catalytic versions, albeit most of them do not meet the criteria of atom economy.[2,3] For this reason allylic oxidative addition of terminal alkenes and carboxylic acids employing Pd^{2+} or Cu^{2+} catalysts has gained considerable interest and is developing as a new tool in natural product synthesis.[4,5] However, a drawback of these methods is that they require a stoichiometric amount of a cooxidant. In order to circumvent this problem we recently invented a redox-neutral process which allows the addition of carboxylic acids to terminal alkynes to furnish branched allylic esters.[6] During the course of this reaction the alkyne serves formally as the oxidant which itself is reduced to the alkene, while a propargylic CH-bond is oxidized. The new transformation is enabled by the presence of a rhodium catalyst derived from $[Rh(COD)Cl]_2$ and the wide bite angle diphosphine DPEphos (**1**).[7] The reaction features a broad substrate scope and a large tolerance regarding functional groups (Scheme 1). Furthermore, an intramolecular variant for atom economic lactone and macrolactone synthesis that avoid high-dilution conditions was developed.[8]

Scheme 1. Redox-Neutral Atom Economic Coupling of Terminal Alkynes with Carboxylic Acids

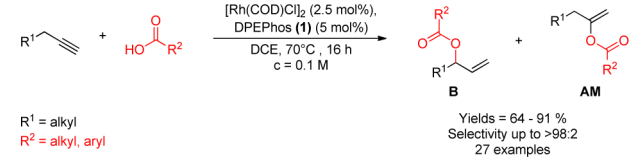

Scheme 2. Control Experiment Employing 3-cyclohexyl-1-propyne (2) or Cyclohexylallene (6) as Substrate

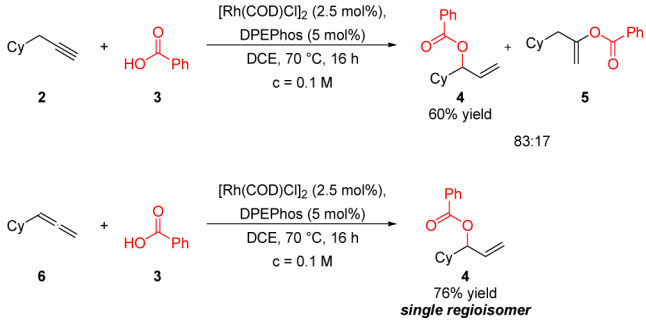

A first hint to a plausible reaction mechanism came from the experiment of terminal alkyne **2** and the isomeric allene **6**. Subjecting both systems to the same reaction conditions in the presence of benzoic acid furnished the same branched allylic ester addition product **4**. In the case of alkyne **2** the Markovnikov addition product **5** was formed as a side product. This was not observed when allene **6** was used as substrate (Scheme 2).

This result allowed us to draw two conclusions: (1) The formation of an allene as an intermediate seems likely; and (2)

Received: November 9, 2013
Published: December 30, 2013

   dx.doi.org/10.1021/ja411204d | *J. Am. Chem. Soc.* 2014, 136, 1097−1104

the side reaction leading to the undesired Markovnikov ester (**5**) occurs before the allene is formed. Based on these ideas, a reaction mechanism was proposed depicted in Scheme 3.[6] Oxidative addition of the carboxylic acid to the Rh(I) (present as monomer **I** or dimer $\mathbf{I}_{dimer}$) leads to the rhodiumhydride species **II**. A subsequent Markovnikov hydrometalation of the terminal alkyne furnishes the vinylrhodium complex **III**. Complex **III** may undergo either reductive elimination resulting in the formation of the observed byproduct **M** or β-hydride elimination to release the allene, proposed as an intermediate of the catalytic transformation based on the results depicted in Scheme 2. A second hydrometalation of the allene by **IV** would form the π-allyl rhodium complex **V**. Reductive elimination should occur at the higher substituted carbon atom and therefore finally liberate the desired branched allylic ester **B** as the main product.[9]

Notably, the observation that an allene displays a higher reactivity compared to the corresponding alkyne (Scheme 2) has enabled the development of an asymmetric version of this reaction starting from terminal allenes.[10]

In order to get a deeper insight into the elementary steps of this new catalytic transformation we performed a thorough mechanistic investigation including NMR and *in*-situ IR spectroscopy as well as ESI-MS investigations. The experiments were supported by rigorous computational studies including state-of-the-art DFT computations.

IN SITU IR SPECTROSCOPIC EXPERIMENTS

We focused on 1-octyne (**7**) and benzoic acid (**3**) as substrates. Because the reaction is extremely air sensitive, we performed kinetic investigations using *in situ* IR spectroscopy under anaerobic conditions. The CO vibration of **8** was clearly distinguishable from that of **3** (Figure 1).

Scheme 3. Proposed Mechanism for the Rhodium Catalyzed Coupling of Terminal Alkynes with Carboxylic Acids

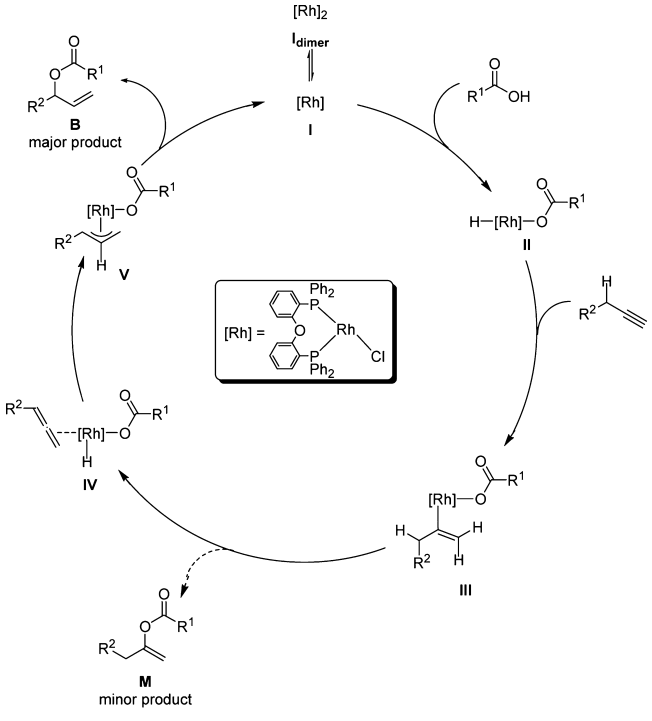

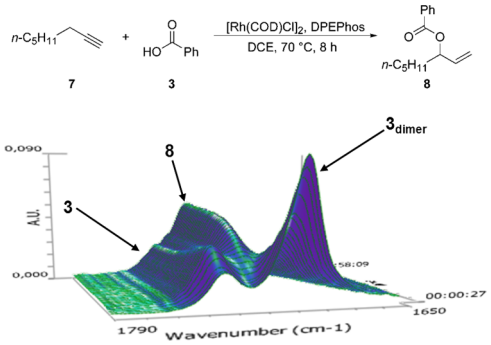

Figure 1. *In-situ* IR spectra of the catalytic transformation. The assignment of the vibrations is based on the IR spectra of isolated **3** and **8** and DFT computations. Conditions: $[Rh(\mathbf{1})Cl]_2$:**7**:**3** = 1:10:10, 70 °C, DCE, c(substrate) = 0.1 M.

Scheme 4. Selectivity Switch Observed by Using the Deuterated Substrate 2-d_2

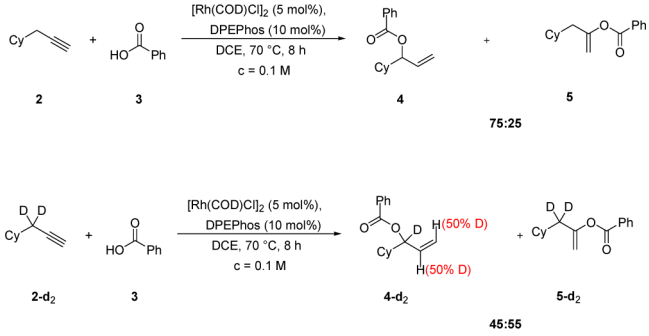

The time-dependent change of the intensity of the CO vibration of **8** was used for a qualitative assignment of the initial reaction rate (for details, see Supporting Information). The first finding was that the reaction rate decreases during the catalysis. To examine a potential dependency of the reaction rate from the concentration of **7**, the increase of the CO vibration of **8** was monitored as a function of the initial amount of **7**. The *in situ*-IR spectroscopic experiments exhibit that the reaction is not accelerated by increasing the concentration of **7**. An analogous kinetic study by varying the amount of **3** was performed. However, higher concentrations of **3** do not increase the reaction rate either. The initial rate studies are consistent with a zero-order dependence on both substrates, although experiments show a decreasing rate of product formation with increasing turnover. Conversely, we find a direct proportionality between the reaction rate and the amount of catalyst, so a first-order dependency on the catalyst concentration could be concluded.

Interestingly, when subjecting the deuterium labeled substrate **2**-d_2 (see Scheme 4) to standard catalysis conditions a selectivity switch toward the formation of the Markovnikov ester (**M** in Scheme 3 and **5**-d_2 in Scheme 4) is observed. Assuming an underlying normal isotope effect, the β-hydride elimination as proposed in Scheme 3 seems to have been slowed down. Accordingly, the reductive elimination step leading to the Markovnikov ester **M** becomes the more favorable pathway. These results further suggest that a rhodium vinyl species (**III** in Scheme 3) is indeed part of the catalytic cycle.

dx.doi.org/10.1021/ja411204d | *J. Am. Chem. Soc.* 2014, 136, 1097−1104

ESI-MS INVESTIGATION

The observed zero order of the reaction rate on the substrate concentrations may be rationalized by assuming that a resting state is present during the catalytic transformation already bearing both substrates in its coordination sphere. By going from such a resting state to the highest transition state, no substrate would enter the catalytic cycle, explaining the observed kinetics. To examine whether such a resting state is detectable, we subjected authentic catalytic solutions to electrospray MS (ESI-MS) analysis. Because of the ease of transferring solution-phase ions to the gas phase for identification or further reactions, ESI-MS has become increasingly popular as a tool for studying short-lived reactive intermediates in organometallic catalytic cycle.[11,12] As only charged species can be detected by means of ESI-MS, we had to ensure that at any time in the course of the catalytic cycle the intermediates of interest are ionic. The use of charge-tagged ligands/substrates has proven to be quite useful for, among others,[13] the mechanistic study of the rhodium catalyzed hydroformylation.[14] Therefore, we synthesized a permanently charged substrate **9** (Scheme 5). Using a charge-tagged substrate instead of charge-tagged ligand has the advantage that ionic products can be detected by means of mass spectrometry.

This way, all intermediates bearing the charged substrate are detectable. In order to monitor the ionic products/intermediates in an online fashion, a solution containing similar reactant and catalyst concentrations (in dichloroethane) to the actual reaction was transferred from a sealed pressurized flask to the electrospray source through a PEEK capillary (for details, see Supporting Information). By this arrangement, the analysis of solutions over a broad pressure range from atmospheric pressure[15] up to 150 bar is possible.[16] The configuration of the mass spectrometer was octopole−quadrupole−octopole−quadrupole (O1/Q1/O2/Q2) as described earlier.[11,12]

Scheme 5. Permanently Charged Alkyne 9 and the Corresponding Charged Product 10

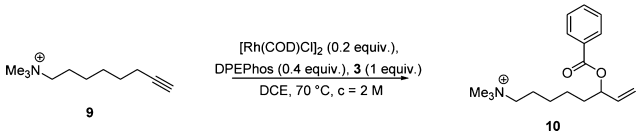

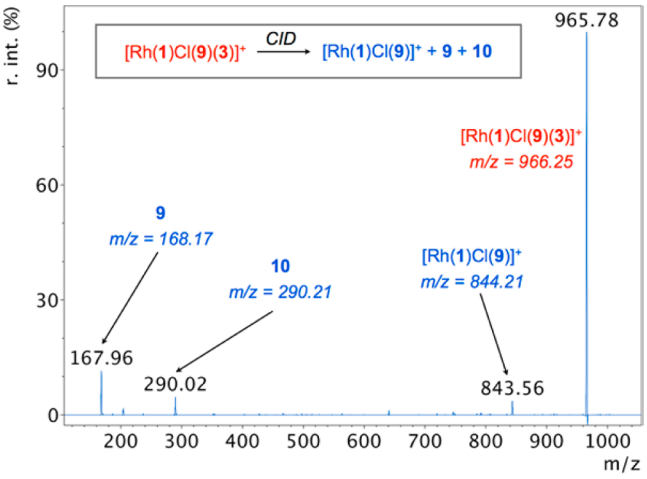

Figure 2. CID with the ion m/z 966.

Charged substrate **9** was used as alkyne compound in our standard catalytic protocol, and the reaction mixture subjected to MS analysis by the PSI method. The formation of charged allylic ester **10** was observed, which shows that the charge tag does not interfere obstructively with the catalyst. Additionally, a species with m/z 844 was observed. This would correspond to a complex where **9** is coordinated to the [Rh(**1**)Cl] fragment. Additionally, a very prominent signal with m/z 966 was present that matches the mass of the [Rh(**1**)Cl] fragment plus substrate **9** plus benzoic acid **3**. In order to assign a structure to this ion, m/z 966 was selected in Q1 and subjected to a CID experiment in O2 (Ar, 1.1 × 10^{-4} mbar, E_{lab} = 30 eV) (Figure 2).

Collision with argon leads, besides the loss of **9**, to a fragment with m/z 290 (i.e., the charge-tagged product **10**), indicating that a catalytic intermediate en route to the product was observed. Hence, the ESI-MS results speak for the reductive elimination step to take place in a unimolecular fashion. Interestingly, another fragment with m/z 844 was detected corresponding to the loss of benzoic acid **3**. The analogous species pattern can be seen when a charge-tagged derivative of hexyne is used as a substrate. It is important to note that the CID experiments (collision energy from 0 to 50 eV) did not result in the formation of a Rh complex either bearing a hydride or benzoate. This means that at variance to the originally proposed mechanism (Scheme 3), the ESI-MS results do not hint to an insertion of the rhodium into the OH bond of benzoic acid **3**. The results of the ESI-MS investigations agree with the kinetic studies since the detected intermediate to which both substrates already coordinate may represent the resting state of the catalytic cycle.

NMR AND X-RAY SPECTROSCOPIC INVESTIGATIONS OF INTERMEDIATES

To examine the molecular nature of this resting state in more detail, we decided to monitor the reaction mixture by NMR spectroscopy. This study commenced with the *in situ* preparation of [Rh(**1**)Cl]$_2$. Indeed, upon reaction of [Rh(COD)Cl]$_2$ and **1** for 20 min at 70 °C, a new doublet at 38.8 ppm was observed in the ^{31}P NMR spectra, displaying a $^{1}J_{Rh-P}$ coupling of 200 Hz, a typical value for μ-Cl bridged dinuclear rhodium complexes.

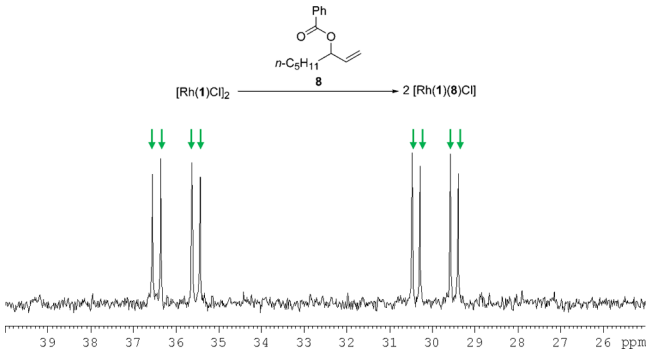

Figure 3. ^{31}P NMR spectrum after the addition of **8** to the isolated [Rh(**1**)Cl]$_2$ complex. The green arrows mark the new ABX spin system.

Initial experiments to identify whether the carboxylic acid (as proposed in the original mechanism) or the alkyne reacts with

dx.doi.org/10.1021/ja411204d | J. Am. Chem. Soc. 2014, 136, 1097−1104

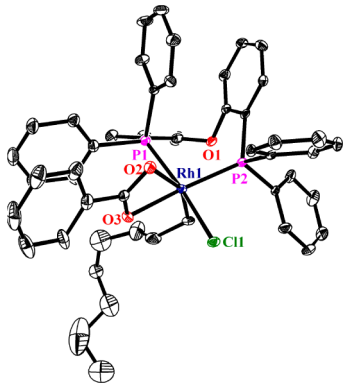

Figure 4. Molecular structure of [Rh(**1**)(σ-allyl)(carboxylate)Cl] (**11**) (ORTEP, 30% probability ellipsoids). Hydrogen atoms were omitted for clarity. Obtained from a mixture of $[Rh(\mathbf{1})Cl]_2$ and allylic ester **8**.

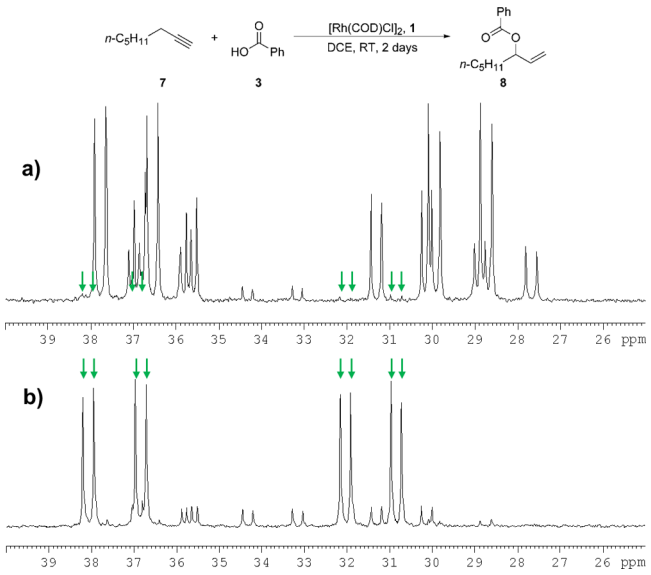

Figure 5. ^{31}P NMR spectrum obtained under normal reaction conditions at room temperature (a) after 30 min and (b) after 2 days. The green arrows mark the two signals of **11**.

$[Rh(\mathbf{1})Cl]_2$ were performed upon addition of the components at room temperature, and the reaction was monitored via ^{31}P NMR spectroscopy. The addition of the benzoic acid **3** did not lead to changes in the ^{31}P NMR spectrum, whereas after addition of the alkyne **7** a new spectral signature was observed. These experiments (for details, see the Supporting Information) clearly indicate that the alkyne reacts first with the neutral dinuclear rhodium complex. While the structure of this initially formed alkyne complex could not be solved yet, this observation that the alkyne reacts first will be important for further mechanistic conclusions.

Since the results obtained by *in situ* IR spectroscopy suggested that an increasing product concentration correlates with a decrease of the reaction rate, the question arose whether this is caused by product inhibition through coordination of the product ester **8** to the rhodium catalyst. To probe this notion, allylic ester **8** was allowed to react with $[Rh(\mathbf{1})Cl]_2$. Indeed a new species was obtained reflected by a new spectral signature in the ^{31}P NMR spectrum (Figure 3).

The new species displays an ABX-spin system with a $^{1}J_{Rh-P}$ coupling of 144.8 and 150 Hz, respectively, and a $^{2}J_{P-P}$ coupling of 35.0 Hz each. Hence, both phosphorus atoms are bound to the same rhodium atom. Repeating this reaction for 1 h at 50 °C yielded substantial amounts of a yellow solid that was recrystallized from THF/hexane. Crystals suitable for X-ray diffraction analysis (Figure 4) were thus obtained. Surprisingly, the crystal structure revealed that the product had undergone an oxidative addition to form an allyl complex. However, the allyl substituent is not bound in a η^3-fashion but rather as a σ-allyl and the carboxylate coordinates as a bidentate ligand. Redissolving these crystals in THF-d_8 provide the same ABX-spin system in the ^{31}P NMR spectrum as shown in Figure 3. Further NMR spectroscopic investigations to clarify the coordination of the carboxylate and the allyl are reported in the Supporting Information and indicate the same coordination as shown in Figure 4.

A reaction carried out with isolated **11** as catalyst under standard conditions (same catalyst loading) gave the branched allylic ester **8** with 66% yield, indicating that **11** is indeed part of the catalytic transformation.

With the knowledge that the product reacts with the active catalyst, we next analyzed the changes in the ^{31}P NMR spectrum during the actual catalytic transformation. In order to be able to detect transient complexes these experiments were conducted at room temperature (Figure 5).

After 30 min at room temperature, at least five distinguishable species are detectable by ^{31}P NMR spectroscopy. Interestingly, at this point no "free" product is observable in the ^{1}H NMR spectrum, but the product complex **11** is already formed. After 2 days at room temperature, **11** becomes the dominant species in the ^{31}P NMR spectrum (Figure 5b). Analysis of the ^{1}H NMR spectrum revealed that only 4% of the "free" product is formed after 2 days at room temperature. These results indicate a high-stability constant of **11** and that the higher reaction temperature of 70 °C is crucial to enable the dissociation of the product complex. On the other hand, since **11** becomes the main species, the stoichiometric reaction starting from the isolated dimer was shown to be possible even at room temperature. These findings altogether indicate that **11** presents the resting state of the catalytic transformation.

The NMR spectroscopic investigations suggest in the first instance a coordination of the alkyne instead of the benzoic acid as described in the originally proposed mechanism. As noted above, at least five rhodium species can be observed after starting the reaction at room temperature. Surprisingly, one of these species is the rhodium complex **11** which is formed if the product (**8**) is available and is temporarily present as main species.

■ COMPUTATIONAL INVESTIGATIONS

In order to support the experimental studies we performed DFT computations to gain an atomistic understanding of the catalytic process. All structures and transition states were optimized using the BP86[17] functional in conjunction with def2-SVP[18] basis set. Single point computations were performed using the same basis set with the meta hybrid M06[19] functional. This level of theory was chosen for the final energy computations since it outperformed the BP86/def2-TZVP,[20] B3LYP[21]/def2-TZVP, PBE0[22]/def2-TZVP, and the M06/def-TZVP levels of theory in benchmark computations against CCSD(T) calculations for a model system in which the ligand **1** was replaced by PH_3 (for details see Supporting Information). All DFT calculations discussed herein were then performed with the ligand **1** without any simplifications. To account for solvent effects the IEFPCM model with the default

dx.doi.org/10.1021/ja411204d | J. Am. Chem. Soc. 2014, 136, 1097−1104

Table 1. Equilibrium Structure of 11 Measured by X-ray Spectroscopy and the Simplified Complex 11 Computed by DFT

	X-ray	BP86/def2-SVP
Rh−C	2.089(3)	2.110
Rh−O3	2.1386(19)	2.158
Rh−O2	2.341(2)	2.380
Rh−P1	2.2930(8)	2.331
Rh−P2	2.2713(8)	2.313
Rh−Cl	2.3983(7)	2.400
P1−Rh−P2	98.33(3)	100.05

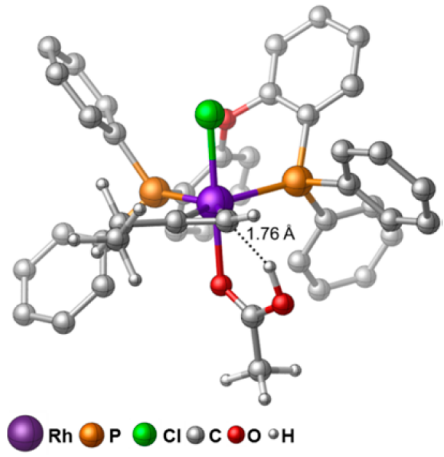

Figure 6. DFT optimized structure of a [Rh(**1**)(acid)(alkyne)Cl] complex exhibiting an unusual C_{sp}···HO hydrogen bond.

Scheme 6. Protonation of the alkyne leading to the rhodium(III) species

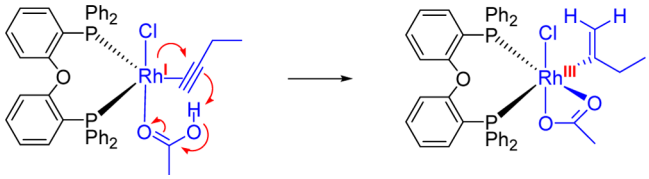

parameters for dichloroethane was applied. All computations were performed using Gaussian 09.[23] Benzoic acid **3** used experimentally was replaced in the computations by acetic acid and the 1-octyne by 1-butyne. In order to check if these simplifications are acceptable, we optimized the structure of complex **11** at the BP86/def2-SVP level of theory and compared it to the structure derived from X-ray analysis.

Indeed, the structural parameters obtained by X-ray analysis are in close agreement to those calculated at the BP86/def2-SVP level. Since the ESI-MS investigations led to the conclusion that a monomeric species is the active catalyst, we assumed monomerization of the $[Rh(\mathbf{1})Cl]_2$ to take place first. Our attempts commenced with calculating the originally proposed catalytic cycle (see Figure 7).[24] However, NMR spectroscopic as well as ESI-MS investigation suggests that the oxidative addition into the OH bond does actually not occur. This finding motivated us to calculate alternative pathways by means of DFT in which the alkyne binds first to the T-shaped [Rh(**1**)Cl] complex, followed by the coordination of the acid. Interestingly, upon optimization of different conformers, one exhibiting an unusual C_{sp}···HO hydrogen bond was found to be lowest in energy (Figure 6).

This intermediate is in a perfect orientation for an intramolecular proton transfer to the C_{sp}-carbon atom. Such a protonation would directly lead to the rhodium(III)-vinyl species proposed as an intermediate based on the observed selectivity switch (see Scheme 6).

This is therefore a rare example where an oxidative addition to a late transition metal is initiated by a protonation of a C_{sp}-carbon in the coordination sphere of the metal center.[25]

Indeed, a reaction sequence involving the [Rh(**1**)(acid)(alkyne)Cl] species and an intramolecular protonation is computed to be lower in energy than the originally proposed reaction sequence (Figure 7).

This intramolecular protonation is followed by the formation of a hydride complex via insertion of the rhodium into the α-CH bond of the vinylidene (β-hydride elimination). Next, the *in situ* generated allene complex is hydrometalated to form an η^3-allyl complex which can undergo reductive elimination to furnish the product **8** (Figure 8). We furthermore investigated the possibility of a solvent coordination to the monomeric [Rh(**1**)Cl] complex. Indeed, a weak Cl−Rh bond stabilizes this 14-electron complex by 5.6 kcal/mol. However, the alkyne coordination to this $[Rh(\mathbf{1})Cl]\cdot C_2H_4Cl_2$ adduct requires an activation energy of 13.8 kcal/mol. Therefore, the dissociative pathway seems to be preferred.

DISCUSSION

An analysis of the potential energy profile depicted in Figure 8 reveals that the monomeric [Rh(**1**)Cl] complex is the intermediate highest in energy formed during the catalytic cycle. This would suggest that the monomerization of the $[Rh(\mathbf{1})Cl]_2$ complex is the rate-determining step. However, such an interpretation would not take into account the "Ouroboros" nature of a catalytic transformation.[26] In addition, it would remain unclear why **11** was identified as resting state of the catalytic cycle. Therefore, the energy surface obtained by DFT computations was rigorously analyzed in terms of the energetic span concept introduced by Kozuch, Shaik, and Martin (Figure 9).[26,27]

By regarding the η^3- or the σ-allyl complex as resting state of the catalytic cycle and going from this species to the next highest transition state in direction of the chemical flow of the catalysis, it appears that the energetic span is determined by the σ-allyl complex **11** and the transition state for the reductive elimination. This is in agreement with the experimentally observed zero-order dependency on the substrate concentrations since no substrate enters or leaves the cycle between the two species determining the energetic span.

On investigating the reductive elimination to the product by DFT computations starting from **11**, it appeared that the transition state is higher in energy than the one corresponding to the η^3-allyl complex (Figure 10). This finding implies a preliminary σ/π-isomerization of the allyl complex followed by the reductive elimination to the product **8**.

We were also able to locate a transition state connecting the η^3-complex and **11** (Figure 11).

The calculated activation energy for this process is lower than the activation energy for the reductive elimination. This shows that the Curtin−Hammett principle can be applied to the reductive elimination step.

dx.doi.org/10.1021/ja411204d | J. Am. Chem. Soc. 2014, 136, 1097−1104

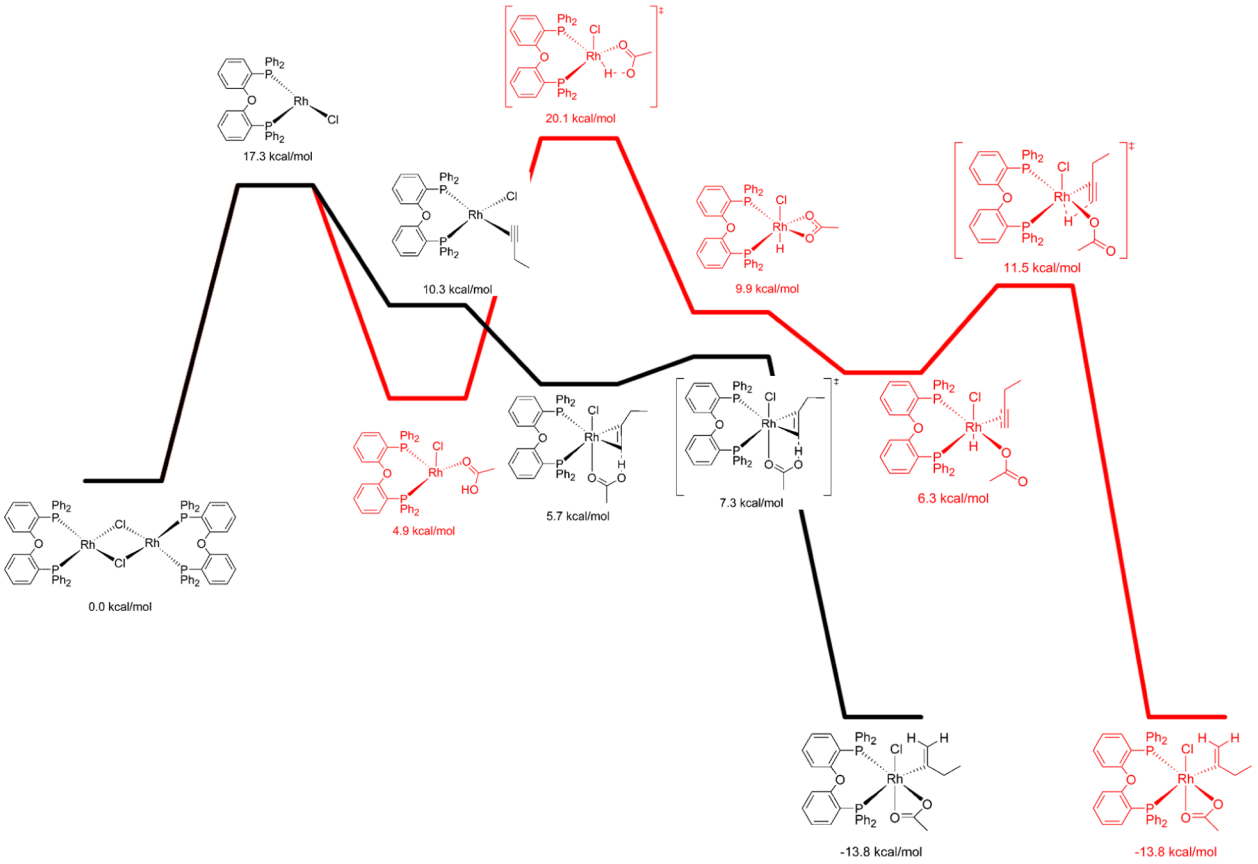

Figure 7. The proposed mechanism (red) and alternative mechanisms (black) involving the formation of an [Rh(**1**)(acid)(alkyne)Cl] species and an intramolecular protonation. All energies are given as the sum of electronic energy and zero point correction (PCM-M06/def2-SVP//BP86/def2-SVP) with respect to the sum of the energies of the $[Rh(\mathbf{1})Cl]_2$ complex and the substrates.

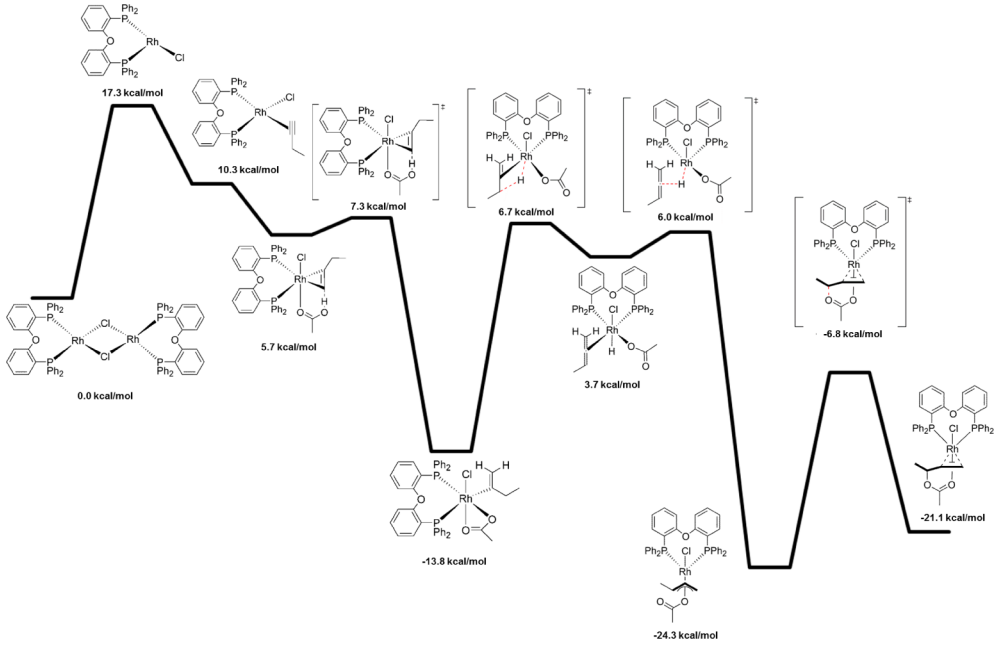

Figure 8. Computed catalytic cycle of the rhodium catalyzed propargylic CH activation. All energies are given as the sum of electronic energy and zero point correction (PCM-M06/def2-SVP//BP86/def2-SVP) with respect to the sum of the energies of the $[Rh(\mathbf{1})Cl]_2$ complex and the substrates.

dx.doi.org/10.1021/ja411204d | *J. Am. Chem. Soc.* 2014, 136, 1097−1104

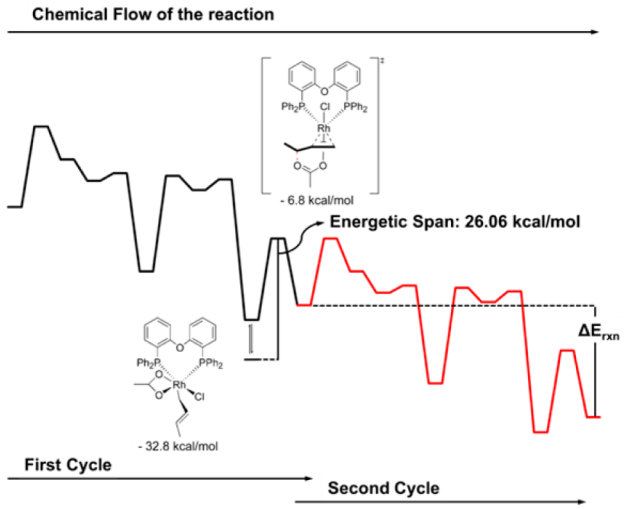

Figure 9. Interpretation of the computed E+zpv profile by means of the energetic span model.

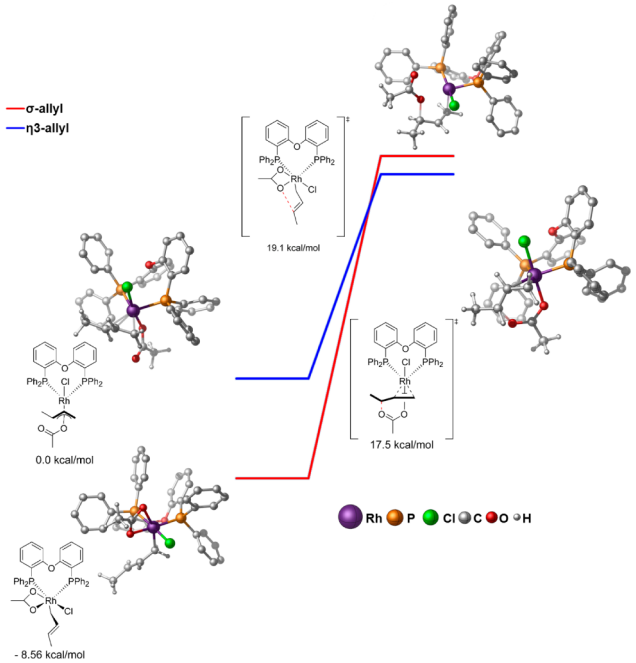

Figure 10. Energy difference of the transition states leading to the product starting from different allyl complexes.

CONCLUSION

All experimental and theoretical results show that the originally postulated mechanism has to be revised. Instead of a rhodium insertion into the OH bond an unusual C_{sp} protonation takes place. A σ-allyl complex was identified as the turn over determining intermediate and thoroughly characterized by means of NMR spectroscopy and X-ray crystallography. A destabilization of this σ-allyl complex by employing a modified ligand would therefore increase the reaction rate. Experimental and computational investigations in order to identify an appropriate ligand are ongoing in our laboratories.

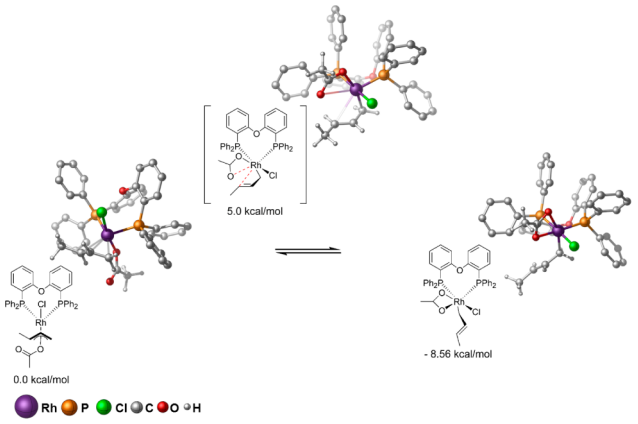

Figure 11. The transition state connecting the η^3- and the σ-allyl complex.

ASSOCIATED CONTENT

Supporting Information

Experimental procedures, kinetic data, *in situ* IR and NMR spectroscopic experiments, X-ray crystallographic and spectroscopic data for new compounds, ESI-MS experimental data, computational details, and Cartesian coordinates of all calculated species. This material is available free of charge via the Internet at http://pubs.acs.org.

AUTHOR INFORMATION

Corresponding Author

bernhard.breit@chemie.uni-freiburg.de

Notes

The authors declare no competing financial interest.

ACKNOWLEDGMENTS

This work was supported by the DFG, the International Research Training Group "Catalysts and Catalytic Reactions for Organic Synthesis"(IRTG 1038), the Fonds der Chemischen Industrie (PhD fellowship to U.G.), and the Krupp Foundation (Alfred-Krupp Award to B. B.). We thank Umicore, BASF, and Wacker for generous gifts of chemicals. We thank PD Dr. Wolfgang Baumann for the characterization of the σ-allyl complex by means of NMR spectroscopy.

REFERENCES

(1) (a) Hodgson, D. M.; Humphreys, P. G. In *Science of Synthesis: Houben-Weyl Methods of Molecular Transformations*; Clayden, J. P., Ed.; Thieme: Stuttgart, Germany, 2007; Vol. *36*, pp 583−665. (b) Lumbroso, A.; Cooke, M. L.; Breit, B. *Angew. Chem.* **2013**, *125*, 1942.

(2) For mercury and selenium catalyzed reactions, see: (a) Rappoport, Z.; Winstein, S.; Young, W. G. *J. Am. Chem. Soc.* **1972**, *94*, 2320−2329. (b) Sharpless, K. B.; Lauer, R. F. *J. Am. Chem. Soc.* **1972**, *94*, 7154−7155. (c) Sharpless, K. B.; Lauer, R. F. *J. Org. Chem.* **1974**, *39*, 429−430.

(3) Trost, B. M. *Angew. Chem., Int. Ed. Engl.* **1995**, *34*, 259−281.

(4) For palladium catalyzed reactions, see: (a) Chen, M. S.; White, M. C. *J. Am. Chem. Soc.* **2004**, *126*, 1346−1347. (b) Chen, M. S.; Prabagaran, N.; Labenz, N. A.; White, M. C. *J. Am. Chem. Soc.* **2005**, *127*, 6970−6971. (c) Mitsudome, T.; Umetani, T.; Nosaka, N.; Mori, K.; Mizugaki, T.; Ebitani, K.; Kaneda, K. *Angew. Chem., Int. Ed.* **2006**, *45*, 481−485. (d) Covell, D. J.; White, M. C. *Angew. Chem., Int. Ed.* **2008**, *47*, 6448−6451. (e) Stang, E. M.; White, M. C. *Nat. Chem.* **2009**, *1*, 547−551. (f) Vermeulen, N. A.; Delcamp, J. H.; White, M. C. *J. Am. Chem. Soc.* **2010**, *132*, 11323−11328. (g) Thiery, E.; Aouf, C.; Belloy, J.; Harakat, D.; Le Bras, J.; Muzart, J. *J. Org. Chem.* **2010**, *75*,

1771−1774. (h) Henderson, W. H.; Check, C. T.; Proust, N.; Stambuli, J. P. *Org. Lett.* **2010**, *12*, 824−827. (i) Campbell, A. N.; White, P. B.; Guzei, I. A.; Stahl, S. S. *J. Am. Chem. Soc.* **2010**, *132*, 15116−15119.

(5) For copper catalyzed reactions, see: (a) Malkov, A. V.; Bella, M.; Langer, V.; Kocovský, P. *Org. Lett.* **2000**, *2*, 3047−3049. (b) Eames, J.; Watkinson, M. *Angew. Chem., Int. Ed.* **2001**, *40*, 3567−3571. (c) Le Bras, J.; Muzart, J. *Tetrahedron Lett.* **2002**, *43*, 431−433. (d) Fache, F.; Piva, O. *Synlett* **2002**, 2035−2036. (e) Andrus, M. B.; Zhou, Z. *J. Am. Chem. Soc.* **2002**, *124*, 8806−8807.

(6) Lumbroso, A.; Koschker, P.; Vautravers, N. R.; Breit, B. *J. Am. Chem. Soc.* **2011**, *133*, 2386−2389.

(7) The bite angle of **1** was determined to be 102.2° with a flexibility range of 86−120°: Kranenburg, M.; van der Burgt, Y. E. M.; Kamer, P. C. J.; van Leeuwen, P. W. N. M. *Organometallics* **1995**, *14*, 3081−3089.

(8) Lumbroso, A.; Abermil, N.; Breit, B. *Chem. Sci.* **2012**, *3*, 789−793.

(9) For the regiochemistry of reductive elimination from late transition-metal complexes see: (a) Hayashi, T.; Okada, A.; Suzuka, T.; Kawatsura, M. *Org. Lett.* **2003**, *5*, 1713−1715. (b) Polet, D.; Alexakis, A.; Tissot-Croset, K.; Corminboeuf, C.; Ditrich, K. *Chem.—Eur. J.* **2006**, *12*, 3596−3609. (c) Vrieze, D. C.; Hoge, G. S.; Hoerter, P. Z.; Van Haitsma, J. T.; Samas, B. M. *Org. Lett.* **2009**, *11*, 3140−3142.

(10) Koschker, P.; Lumbroso, A.; Breit, B. *J. Am. Chem. Soc.* **2011**, *133*, 20746−20749.

(11) Plattner, D. A. *J. Mass Spectrom.* **2001**, *207*, 125 and the references therein.

(12) Plattner, D. A. *Top. Curr. Chem.* **2003**, *225*, 153 and the references therein.

(13) Chisholm, D. M.; McIndoe, J. S. *Dalton Trans.* **2008**, 3933−3945.

(14) Beierlein, C. H.; Breit, B.; Paz Schmidt, R. A.; Plattner, D. A. *Organometallics* **2010**, *29*, 2521−2532.

(15) Vikse, K. L.; Ahmadi, Z.; Luo, J. W.; van der Wal, N.; Daze, K.; Taylor, N.; McIndoe, J. S. *Int. J. Mass Spectrom.* **2012**, *323*, 8−13.

(16) Paz-Schmidt, R. A.; Bonrath, W.; Plattner, D. A. *Anal. Chem.* **2009**, *81*, 3665−3668.

(17) Becke, A. D. *Phys. Rev. A* **1988**, *38*, 3098−3100. Perdew, J. P. *Phys. Rev. B* **1986**, *33*, 8822−8824.

(18) Weigend, F.; Ahlrichs, R. *Phys. Chem. Chem. Phys.* **2005**, *7*, 3297−3305.

(19) Zhao, Y.; Truhlar, D. G. *Theor. Chem. Acc.* **2008**, *120*, 215−241.

(20) Weigend, F.; Ahlrichs, R. *Phys. Chem. Chem. Phys.* **2005**, *7*, 3297−3305.

(21) Becke, A. D. *J. Chem. Phys.* **1993**, *98*, 5648−5652.

(22) Adamo, C.; Barone, V. *J. Chem. Phys.* **1999**, *110*, 6158−6170.

(23) Frisch, M. J.; Trucks, G. W.; Schlegel, H. B.; Scuseria, G. E.; Robb, M. A.; Cheeseman, J. R.; Scalmani, G.; Barone, V.; Mennucci, B.; Petersson, G. A.; Nakatsuji, H.; Caricato, M.; Li, X.; Hratchian, H. P.; Izmaylov, A. F.; Bloino, J.; Zheng, G.; Sonnenberg, J. L.; Hada, M.; Ehara, M.; Toyota, K.; Fukuda, R.; Hasegawa, J.; Ishida, M.; Nakajima, T.; Honda, Y.; Kitao, O.; Nakai, H.; Vreven, T.; Montgomery, J. A., Jr.; Peralta, J. E.; Ogliaro, F.; Bearpark, M.; Heyd, J. J.; Brothers, E.; Kudin, K. N.; Staroverov, V. N.; Kobayashi, R.; Normand, J.; Raghavachari, K.; Rendell, A.; Burant, J. C.; Iyengar, S. S.; Tomasi, J.; Cossi, M.; Rega, N.; Millam, N. J.; Klene, M.; Knox, J. E.; Cross, J. B.; Bakken, V.; Adamo, C.; Jaramillo, J.; Gomperts, R.; Stratmann, R. E.; Yazyev, O.; Austin, A. J.; Cammi, R.; Pomelli, C.; Ochterski, J. W.; Martin, R. L.; Morokuma, K.; Zakrzewski, V. G.; Voth, G. A.; Salvador, P.; Dannenberg, J. J.; Dapprich, S.; Daniels, A. D.; Farkas, Ö.; Foresman, J. B.; Ortiz, J. V.; Cioslowski, J.; Fox, D. J. *Gaussian 09*, rev. B.01; Gaussian, Inc.: Wallingford, CT, 2010.

(24) In addition, we computed an alternative pathway leading to the allene by rhodium insertion into the α-CH bond of the alkyne followed by a subsequent hydrometalation. However, the calculated barrier of this process renders it unlikely to occur. Details are reported in the Supporting Information.

(25) A similar "oxidative protonation" of a rhodium complex bearing an alkyne in the coordination sphere leading to a rhodium vinyl complex was reported by Wolf and Werner: Wolf, J.; Werner, H. *Organometallics* **1987**, *6*, 1164−1169.

(26) (a) Kozuch, S.; Shaik, S. *J. Am. Chem. Soc.* **2006**, *128*, 3355−3365. (b) Kozuch, S.; Shaik, S. *Acc. Chem. Res.* **2011**, *44*, 101−110.

(27) Kozuch, S.; Martin, J. M. L. *ChemPhysChem.* **2011**, *12*, 1413−1418.